

RSC Advances



This is an *Accepted Manuscript*, which has been through the Royal Society of Chemistry peer review process and has been accepted for publication.

Accepted Manuscripts are published online shortly after acceptance, before technical editing, formatting and proof reading. Using this free service, authors can make their results available to the community, in citable form, before we publish the edited article. This *Accepted Manuscript* will be replaced by the edited, formatted and paginated article as soon as this is available.

You can find more information about *Accepted Manuscripts* in the [Information for Authors](#).

Please note that technical editing may introduce minor changes to the text and/or graphics, which may alter content. The journal's standard [Terms & Conditions](#) and the [Ethical guidelines](#) still apply. In no event shall the Royal Society of Chemistry be held responsible for any errors or omissions in this *Accepted Manuscript* or any consequences arising from the use of any information it contains.

Anomalous mechanical strengths and shear deformation paths of Al_2O_3 polymorphs with high ionicity

Z. Zhang,^{1,2} Z. H. Fu,^{1,2} R. F. Zhang,^{1,2,*} D. Legut,³ and H. B. Guo^{1,*}

¹*School of Materials Science and Engineering, Beihang University, Beijing 100191, P. R. China*

²*Center for Integrated Computational Engineering, International Research Institute for Multidisciplinary Science, Beihang University, Beijing 100191, P. R. China*

³*IT4 Innovations Center, VSB-Technical University of Ostrava, CZ-70833 Ostrava, Czech Republic; Charles University, Faculty of Mathematics and Physics, Department of Condensed Matter Physics, KeKarlovu 5, CZ-12 116 Prague 2, Czech Republic*

Abstract

Alumina formed by selective oxidization provides an effective way to protect aluminide alloys against corrosion for sustainable applications. Despite a broad interest and investigations on Al_2O_3 polymorphs such as $\alpha\text{-Al}_2\text{O}_3$ and $\theta\text{-Al}_2\text{O}_3$, their intrinsically mechanical strengths and atomic deformation mechanism have not yet been fully understood. Here using density functional theory, we show that the calculated shear moduli and mechanical strengths of $\theta\text{-Al}_2\text{O}_3$ are substantially lower than those of $\alpha\text{-Al}_2\text{O}_3$, explaining why $\theta\text{-Al}_2\text{O}_3$ is much weaker than $\alpha\text{-Al}_2\text{O}_3$. An analysis of shear deformation paths and electronic structure indicates that the longest Al-O ionic bonds are responsible for the lattice instability of both polymorphs during shear, showing however a different anisotropic feature. This study sheds a novel view on the failure of thermally grown $\alpha\text{-Al}_2\text{O}_3$ and $\theta\text{-Al}_2\text{O}_3$, and it should help to improve the performance of thermal barrier coatings.

* Author to whom correspondence should be addressed: zrf@buaa.edu.cn and guo.hongbo@buaa.edu.cn

I. INTRODUCTION

Alumina polymorphs are important ceramic materials with many desirable properties such as high hardness, chemical inertness, thermal shock resistance and wear resistance, which brought them many technological applications such as protective coatings, abrasives, insulators, and catalysts [1-4]. The most stable form of alumina is α -Al₂O₃ which is termed as a quasi-harmonic crystal with negligible intrinsic anharmonic effects [5]. Beside of the α -Al₂O₃, alumina may adopt a series of metastable transition polymorphs such as γ , η , θ , γ' , and δ structures with different fcc packing of oxygen, and α , κ , κ' , and ι structures based on hcp packing lattice [6,7]. Some other structures include θ' , θ'' , λ , U and χ are also reported in publications [6,7]. When Al₂O₃ adopts the fcc packing lattice, a phase transformation of alumina may appear in the following four sequences [7]:

- i) γ -AlO(OH) (Boehmite) $\xrightarrow{300^{\circ}\text{--}500^{\circ}\text{C}}$ γ $\xrightarrow{700^{\circ}\text{--}800^{\circ}\text{C}}$ δ $\xrightarrow{900^{\circ}\text{--}1000^{\circ}\text{C}}$ θ $\xrightarrow{1000^{\circ}\text{--}1100^{\circ}\text{C}}$ α -Al₂O₃
- ii) α -Al(OH)₃ (Bayerite) $\xrightarrow{200^{\circ}\text{--}300^{\circ}\text{C}}$ η $\xrightarrow{600^{\circ}\text{--}800^{\circ}\text{C}}$ θ $\xrightarrow{1000^{\circ}\text{--}1100^{\circ}\text{C}}$ α -Al₂O₃
- iii) Amorphous (Anodic film) $\rightarrow \gamma \rightarrow \delta \rightarrow \theta \rightarrow \alpha$ -Al₂O₃
- iv) Melt $\rightarrow \gamma \rightarrow \delta, \theta \rightarrow \alpha$ -Al₂O₃

With these alumina polymorphs and hydroxides as input, Peintinger et al. [6] systematically investigated their relative stability by means of the hybrid density functional theory, and then obtained the following energetic order: gibbsite < bayerite < boehmite < akdalaite < α -Al₂O₃ < κ -Al₂O₃ < θ -Al₂O₃ < δ -Al₂O₃ < γ -Al₂O₃ < η -Al₂O₃ < ι -Al₂O₃. Lee et al. [8] compared the band gap of some alumina and provided an order of $\alpha > \kappa > \theta > \gamma$, which is agreement with the most recent results by

Museur et al. [9].

Among these alumina polymorphs, the α -Al₂O₃ and κ -Al₂O₃ are used as wear protective coatings on tools due to their superior mechanical properties, whereas the metastable γ -Al₂O₃ and θ -Al₂O₃ are used as catalytic supports because of their lower surface energy [10]. It is generally known that the α - and θ -Al₂O₃ play an important role on the performance of the early oxidation of Ni-Al alloys in thermal barrier coatings (TBCs), whereas the others are generally regarded as defectively metastable ones [11-13]. However, the stress concentration due to the fast phase transformation of θ - to α -Al₂O₃ is an essential factor that leads to the alumina scale cracking and spallation at Al₂O₃/alloy interface in the TBCs [14,15]. To better understand the effect of metastable θ -Al₂O₃ on the performance of TBCs, much effort has been accordingly made to evaluate the properties of θ -Al₂O₃ in experiments and theoretical calculations. However, only limited equilibrium data, such as structural stability, electronic structure and elastic constants have been reported so far. Therefore in the present study, we shall take the former two polymorphs as our focused ones. In the previous theoretical studies, the band gaps of α -Al₂O₃ are calculated to be about 6.72 eV [8], 6.1 eV [16] and 6.24 eV [17], which underestimate the experimental value of 8.8 eV [16,18]. The indirect band gaps of 5.04 eV [8] and 4.98 eV [17] are also reported for θ -Al₂O₃, which are about 1.3-1.7eV smaller than that of α -Al₂O₃. Although the calculated site- and orbital-resolved partial electronic density of states (EDOS) show profound dependence on local coordination of Al and O atoms, the derived effective charge and bond order show similarity for both θ -Al₂O₃ and α -Al₂O₃.

[17]. These results evoke a fundamental question whether both polymorphs could possess a comparable mechanical property.

For this purpose, a comparatively mechanical test of α -Al₂O₃ and θ -Al₂O₃ was performed by Shang et al. [19] several years ago. They obtained a positive value of C_{14} for α -Al₂O₃ by means of *ab initio* DFT calculations, in good agreement with the previous experiments and theoretical studies by Gladden et al. [20] and Hovis et al. [21]. With this validation, the derived bulk moduli and shear moduli of α -Al₂O₃ are shown to be much higher than those of θ -Al₂O₃, providing a guidance for the understanding of the failure origin of TBCs. In Shang's latter work [22], the calculated temperature-dependent elastic constants enable a more realistic stress analysis at elevated temperatures in thermally grown oxides containing α - and θ -Al₂O₃, which provide a deeper understanding of the failure of TBCs in gas-turbine engines.

Although numerous investigations have been performed on the structure and elastic properties of Al₂O₃ polymorphs, relatively little work has been devoted to the calculations of ideal strength and deformation paths which are critical for an in-depth understanding of the failure of turbine parts operating under extreme conditions. In general, a higher elastic modulus does not guarantee a higher strength since the former one describes only the reversible response of a crystal to a small strain, whereas the ideal strength gives an upper limit of stress that an ideal crystal can sustain at large strain [23,24]. In the present paper, we shall take α -Al₂O₃ and θ -Al₂O₃ polymorphs as an illustrative one to show that although both are experimentally

accessible and have similar effective charge and iconicity [17], their mechanical strengths and shear deformation paths are substantially different.

Recent advancement of computational techniques has made it a routine method to calculate the ideal strengths in a reasonable precise by means of first principles methods and provided a way to analyze the deformation paths and electronic instabilities under various loadings [23,25,26]. It is generally recognized that the ideal strength is a fundamental indicator of material strength [27], which is defined as the minimum stress required to plastically deform an ideal crystal and the stress required for the formation of stacking faults [28]. A close connection between Peierls-Nabarro (PN) stress of dislocations and ideal shear strength has also made it possible to evaluate the mechanical strength of a real material via a comprehensive analysis of two intrinsic mechanical parameters: shear moduli and shear strength [25,29]. In addition, the ideal shear strength has attracted much more attention with the progress of nanotechnology, which provides a way to quantitatively measure the near ideal strength which can be obtained from modern first principles calculations [27,30].

II. COMPUTATIONAL METHODS

The *ab initio* density functional theory (DFT) calculations [31,32] were performed using the Vienna *ab initio* simulation package (VASP) code with the Perdew-Burke-Ernzerhof (PBE) [33] version of Generalized Gradient Approximation (GGA) for exchange-correlation functional. For the electronic density of states (EDOS) calculations, we chose the screened hybrid functional of Heyd, Scuseria, and

Ernzerhof (HSE06) [34], where correlation is described in GGA (PBE) and the exchange is a mixture of 25% exact (HF) exchange and 75% PBE exchange. The integration in the Brillouin zone was done on special k points of $9 \times 9 \times 9$ grids for the phases under consideration, energy cutoff of 600 eV, which was sufficient to keep total energy convergence at 10^{-3} meV/atom or less. Atomic positions are relaxed using the conjugate gradient method until the forces on all the atoms were converged to less than 10^{-3} eV/Å.

As a further check of the validity of the applied PAW-PBE potentials, we determine the elastic constants and moduli by applying a set of small deformations δ between -0.02 and +0.02, and calculate the second order coefficients in a polynomial fit of the total energy as a function of the distortion δ . Atomic relaxations were allowed when straining the cell. The applied strain configurations and the corresponding strain-energy density variations $\Delta E/V_0$ for hcp α -Al₂O₃ structure are given as follows: $\varepsilon=(\delta,\delta,0,0,0,0)$ with $\Delta E/V_0=(C_{11}+C_{12})\delta^2$, $\varepsilon=(0,0,0,0,0,\delta)$ with $\Delta E/V_0=1/4(C_{11}-C_{12})\delta^2$, $\varepsilon=(0,0,\delta,0,0,0)$ with $\Delta E/V_0=1/2C_{33}\delta^2$, $\varepsilon=(0,0,0,\delta,0,0)$ with $\Delta E/V_0=1/2C_{44}\delta^2$, and $\varepsilon=(\delta,\delta,\delta,0,0,0)$ with $\Delta E/V_0=(C_{11}+C_{12}+2C_{13}+1/2C_{33})\delta^2$. For θ -Al₂O₃, $\varepsilon=(\delta,0,0,0,0,0)$ with $\Delta E/V_0=1/2C_{11}\delta^2$, $\varepsilon=(0,\delta,0,0,0,0)$ with $\Delta E/V_0=1/2C_{22}\delta^2$, $\varepsilon=(0,0,\delta,0,0,0)$ with $\Delta E/V_0=1/2C_{33}\delta^2$, $\varepsilon=(0,0,0,\delta,0,0)$ with $\Delta E/V_0=1/2C_{44}\delta^2$, $\varepsilon=(0,0,0,0,\delta,0)$ with $\Delta E/V_0=1/2C_{55}\delta^2$, $\varepsilon=(0,0,0,0,0,\delta)$ with $\Delta E/V_0=1/2C_{66}\delta^2$, $\varepsilon=(\delta,\delta,0,0,0,0)$ with $\Delta E/V_0=(1/2C_{11}+C_{12}+1/2C_{22})\delta^2$, $\varepsilon=(\delta,0,\delta,0,0,0)$ with $\Delta E/V_0=(1/2C_{11}+C_{13}+1/2C_{33})\delta^2$.

The *ab initio* DFT calculations of stress-strain dependences conducted here are

technically similar to our previous studies [35-39] to which we refer for further details. The atomic basis vectors of a given unit cell were firstly projected onto the Cartesian coordinate system with one cell axis vector being parallel to the strain direction for the tension loading. In case of shear deformation, one cell axis vector was perpendicular to the slip plane and another one was parallel to the slip direction in that plane. Afterwards, the crystal has been incrementally deformed by transforming the unstrained cell basis vector matrices to the strained ones using the deformation matrices. In order to keep the crystal under a stress state of uniaxial tension or shear, the strained cell has been relaxed for both the cell basis vectors and for the atom position inside the unit cell by keeping the applied strain component fixed and relaxing the other five strain components until their conjugate stress components i.e., Hellmann-Feynman stresses reached negligible values.

III. RESULTS AND DISCUSSION

The α -Al₂O₃ with a space group of *R-3c* has the most symmetric ordering of Al atoms, which leads a higher density compared to other polymorphs. The relaxed topological bond structure of α -Al₂O₃ is shown in Fig. 1(a), the Al cations and the O anions are located at 12c (0, 0, z) and 18e (x, 0, 0.25) Wyckoff positions, respectively. The obtained values of the x- and z-coordinate are 0.306 and 0.352, which are in good agreement with the previous results (x=0.306 and z=0.347) [40]. The α -Al₂O₃ can also be represented in a hexagonal lattice with six layers of close-packed O atoms filled by Al atoms at the octahedral holes sites. Each Al atom is bonded to six O atoms with

two nonequivalent bond distances, and each O atom has four neighbor Al atoms [see Fig. 1(b)]. Figure 1(c) shows the crystal structure and local coordination of anions of θ -Al₂O₃ that belong to monoclinic system with a space group of $C2/m$, with all the ions located at 4i (x, 0, z) Wyckoff positions. Our calculated coordinates of O are: (0.160 0 0.109), (0.495 0 0.257), (0.826 0 0.433), and those of Al: (0.090 0 0.796) (0.342 0 0.683), being in agreement with the previous values of O: (0.163 0 0.123), (0.489 0 0.261), (0.830 0 0.439) and those of Al: (0.101 0 0.794) (0.352 0 0.687) [41]. The Al atoms occupy four octahedral and four tetrahedral interstitials of O sublattice [42] [see Fig. 1(d) and (e)]. The calculated lattice parameters of α -Al₂O₃ are a=4.806Å, c/a=2.7285 and those of θ -Al₂O₃ are a=11.922Å, b=2.940Å, c=5.668Å, β =104.0°. They are in agreement with the available theoretical and experimental values (a=4.8195Å^a, 5.180Å^b, c/a=2.7284^a for α -Al₂O₃ and a=11.923Å^b, 11.8530^c; b=2.941Å^b, 2.904^c; c=5.671Å^b, 5.622^c, β =103.90^{ob}, 103.8^{oc} for θ -Al₂O₃) (^a Ref. [43], ^b Ref. [19], ^c Ref. [44]). There is only one type of O coordination in α -Al₂O₃, but θ -Al₂O₃ has three different types of O coordinations which produce a more complicated bond anisotropy. Figure 1(c) shows that O₁ is bonded to one Al_{tet} and three Al_{oct} cations, where Al_{oct} (Al_{tet}) stands for the Al in octahedral (tetrahedral) coordination. One further see in that figure that O₂ is bonded to two Al_{tet} and one Al_{oct} cations, and O₃ is bonded to one Al_{tet} and two Al_{oct} cations [17]. The Al-O bond lengths of 1.9901 (1.969^d) Å and 1.8730 (1.857^d) Å (^d Ref. [17]) for α -Al₂O₃ [see Fig. 1(b)] show some difference from those of θ -Al₂O₃ in which seven in equivalent Al-O bond lengths are 1.7701, 1.7702, 1.8134, 1.8881, 1.8883, 1.9566, 2.0208 Å [see Fig.

1(d) and (e)], in agreement with the previous values of 1.710, 1.745, 1.896, 1.904, 1.936, 2.025 Å^d (d Ref. [17]) respectively. The difference of local coordination between α -Al₂O₃ and θ -Al₂O₃, especially the bond anisotropy and the longest Al-O bonds are responsible for the different mechanical properties and the deformation paths during shear, as it will be shown.

Based on the reaction $4\text{Al} + 3\text{O}_2 = 2\text{Al}_2\text{O}_3$, the calculated energy difference per formula unit between α - and θ -Al₂O₃ is 0.047 eV, which is consistent with previous reports where the following values were reported $\Delta E(\theta-\alpha)=0.03$ eV/formula unit in Ref. [42] and 0.04 eV/formula unit in Ref. [45] thus confirming that α -Al₂O₃ is thermodynamically more stable than θ -Al₂O₃.

The elastic constants were determined by applying an appropriate set of distortions within elastic limits [46,47]. Table 1 shows the calculated and measured values of the elastic constants C_{ij} for α -Al₂O₃ and θ -Al₂O₃, respectively. The elastic constants satisfy the Born stability criteria [43,48,49], thus confirming that both hexagonal α -Al₂O₃ and monoclinic θ -Al₂O₃ are mechanically stable. Voigt average bulk modulus of B_V of α -Al₂O₃ (235.6 GPa) is much larger than that of θ -Al₂O₃ (187.4 GPa), i.e. the former alumina is more incompressible than the latter one. Additionally, it is found that the anisotropy ratio between C_{11} and C_{33} is nearly unity for α -Al₂O₃, while it is about 1.5 for θ -Al₂O₃, suggesting a higher elastic anisotropy for the latter one. A well-established consideration of whether a crystalline solid is intrinsically ductile or brittle [50-52] can be approximately characterized by the ratio of the shear modulus to the bulk modulus, G/B , by considering B as the resistance to fracture and

G the resistance to plastic deformation [52-54]. The critical G/B ratio which separates ductile and brittle materials is around 0.57, i.e., if $G/B < 0.57$ the material behaves in a ductile manner, otherwise the material is brittle. The relatively high ratio of $G/B \approx 0.63$ for α -Al₂O₃ reveals that it is intrinsically brittle, in agreement with the experiments. The somewhat lower value of 0.58 for θ -Al₂O₃ is closer to the boundary brittle/ductile.

We next investigate the ideal strengths of both Al₂O₃ polymorphs. For α -Al₂O₃, the *ab initio* DFT calculations were performed with unit cell along $\langle 0001 \rangle$, $\langle \bar{1}2\bar{1}0 \rangle$ and $\langle 10\bar{1}0 \rangle$ directions for tension and on $(0001)\langle \bar{1}2\bar{1}0 \rangle$, $(0001)\langle 10\bar{1}0 \rangle$ and $(10\bar{1}0)\langle \bar{1}2\bar{1}0 \rangle$ slip systems for shear. The crystallographic directions of $\langle 010 \rangle$ and $\langle 001 \rangle$ of monoclinic θ -Al₂O₃ are chosen to be parallel to the y and z axes in Cartesian coordinate system respectively. Figure 2(a) shows the calculated stress-strain curves for α -Al₂O₃. The ideal tensile strength of α -Al₂O₃ along the $\langle 0001 \rangle$ direction of about 58.3 GPa is much larger than in the two other directions. The anisotropy ratio of tensile strengths for α -Al₂O₃ of $\sigma_{\langle 0001 \rangle} = 58.3$: $\sigma_{\langle 10\bar{1}0 \rangle} = 36.5$: $\sigma_{\langle \bar{1}2\bar{1}0 \rangle} = 26.3$ GPa $\approx 2.22:1.39:1$ is slightly larger than those of θ -Al₂O₃ [see Fig. 2(b)]: $\sigma_{\langle 010 \rangle} = 28.9$: $\sigma_{\langle 001 \rangle \text{normal}} = 14.8$: $\sigma_{\langle 100 \rangle} = 13.9$ GPa $\approx 2.08:1.06:1$. It is interestingly noted that the anisotropy of ideal tensile strengths does not follow the aforementioned elastic anisotropy for both Al₂O₃ polymorphs. The tensile strength of 26.3 GPa along weakest $\langle \bar{1}2\bar{1}0 \rangle$ direction of α -Al₂O₃ is comparable to the maximum value of 28.9 GPa of θ -Al₂O₃ along the $\langle 010 \rangle$ direction. Because plastic deformation occurs in shear, one must compare the calculated anisotropic ideal shear strengths [35, 36, 55,

56]. The lowest shear strengths of 14.4 GPa of α -Al₂O₃ is found in the (0001)< $\bar{1}2\bar{1}0$ > slip system [Fig. 2(a)]. This value is about 67% higher than the lowest shear strength of 4.7 GPa found for θ -Al₂O₃ [Fig. 2(b)], providing a direct theoretical evidence that θ -Al₂O₃ is intrinsically much weaker than α -Al₂O₃.

As a further understanding of the deformation paths of both Al₂O₃ polymorphs in shear, the change of Al-O bond length and valence charge density differences (VCDD) during shear deformation are compared in Fig. 3. The VCDD is defined as the difference between the calculated total valence charge density of the crystal minus the superposition of the valence charge densities of neutral atoms [39]). Negative value (yellow color in Fig. 3) means a depletion of charges as compared to neutral atoms (bond weakening). To emphasize the variation of charge depletion between Al-O bonds, we show only the negative isosurface of VCDD in Fig. 3. Note that the expansion of negative VCDD isosurface between Al-O bonds indicates their weakening during shear deformations. Although both α -Al₂O₃ and θ -Al₂O₃ have similar ionic bonds, their bond deformation paths and electronic instability modes are substantially different as seen from the change of bond topology and deformed VCDD isosurfaces shown in Figure 3. Figure 3(b) and 3(c) show the typical Al-O bond length and VCDD at shear strain of $\gamma=0.1934$ (before) and $\gamma=0.3400$ (after instability) for α -Al₂O₃, and Fig. 3(e) and 3(f) show them at shear strain of $\gamma=0.0924$ (before) and $\gamma=0.1366$ (after instability) for θ -Al₂O₃. In case of α -Al₂O₃, the shear instability occurs between Al {0001} and O {0001} planes [Fig. 3(b) and 3(c)] with an increase of Al-O bond length from 2.33 to 3.04 Å, whereas in case of θ -Al₂O₃, the shear

instability appears between Al/O {001} planes with the Al-O bond lengths increasing from 2.23 to 2.73 Å [Fig. 3(e) and 3(f)]. In Figure 3, it can also be seen that the dramatic change of VCDD before and after instability of α -Al₂O₃ and θ -Al₂O₃ (see the yellow isosurface marked by big blue arrows), which shows the process of Al-O bond strength becomes weak to bond cleavage.

To quantify the electronic origin of distinct mechanical strength in both Al₂O₃, we first use the quantum theory of atoms in molecules proposed by Bader [57,58] to quantitatively analyze the change of charge transfer during shearing. The calculated nonequivalent values of Bader charges are presented as below: For α -Al₂O₃, at equilibrium: (Al^{-2.4751})₂(O^{+1.6501})₃, at $\gamma=0.1934$ (before instability): (Al^{-2.4732})₂(O^{+1.6488})₃, at $\gamma=0.3400$ (after instability): (Al^{-2.4640})₂(O^{+1.6427})₃; For θ -Al₂O₃, at equilibrium: (Al^{-2.4442/-2.4637})₂(O^{+1.6431/+1.6346/+1.6303})₃, at $\gamma=0.0924$ (before instability): (Al^{-2.4451/-2.4749})₂(O^{+1.6481/+1.6359/+1.6360})₃, at $\gamma=0.1366$ (after instability): (Al^{-2.4479/-2.4733})₂(O^{+1.6340/+1.6442/+1.6431})₃. It is seen that the highly ionicity of α -Al₂O₃ and θ -Al₂O₃ are nearly identical. The minor difference of Bader charges between α - and θ -Al₂O₃ provides an electronic message to be related to the significant differences of their ideal tensile and shear strengths. Further consideration of the distributions of nonequivalent highly ionic Al-O bonds for θ -Al₂O₃, we may get an explanation on the choice of deformation paths of both structures during the shear loadings (see the change of bond lengths and VCDD isosurface marked in Fig. 3).

In order to develop a deeper understanding of the mechanical properties of α -Al₂O₃ and θ -Al₂O₃, we next to analyze the electronic density of states (EDOS) and

localized charge accumulation between Al-O bonds. Fig. 4(a) and (b) shows the total EDOS which presents three distinct regions: the lower part of the valence bands is dominated by O 2s states and the upper part by O 2p- and Al 3s-, 3p-like states. Both α -Al₂O₃ [Fig. 4(a)] and θ -Al₂O₃ [Fig. 4(b)] are insulators with band gaps of about 7.6 and 6.2 eV, respectively. The previously calculated band gaps of α -Al₂O₃ are 8.6 eV [6], 9.1 eV [59], and 8.5 eV [60], and that of θ -Al₂O₃ is 6.9 eV [6], by utilizing HSE functional. A higher value of the band gaps of α -Al₂O₃ was reported in Ref. [59] due to the Hartree-Fock mixing parameter in HSE calculation is 32 %, higher than the standard HSE06 (25 %). Note that the calculated band gap for α -Al₂O₃ by HSE06 pseudopotentials is much more close to the experimental values (~8.8eV) as compared to the previous studies [16,18]. The upper valence band width (from -7.5 eV to 0 eV) of α -Al₂O₃, which is dominated by overlapping of O 2p and Al 3p orbitals, shows strong similarity to θ -Al₂O₃. To get the difference of bond strength between α -Al₂O₃ and θ -Al₂O₃, Fig. 4(c) and 4(d) show the contour plot of the VCDD cross section for α -Al₂O₃ and θ -Al₂O₃. The circled regions between the longest Al-O bonds in Fig. 4(c) and 4(d) indicate the magnitude of charge depletion. It can be clearly seen that the longer Al-O bonds for θ -Al₂O₃ corresponds to a higher depletion of valence charge density between them and a significant bond weakening, providing a physical explanation why α -Al₂O₃ is stronger than θ -Al₂O₃.

IV. CONCLUSIONS

In conclusion, we have studied the structural, thermodynamic, mechanical,

electronic properties and shear deformation paths of α -Al₂O₃ and θ -Al₂O₃ by means of *ab initio* DFT calculations. The resulting equilibrium properties of α -Al₂O₃ and θ -Al₂O₃ are consistent with the experimental and theoretical data. The relatively high bulk modulus of α -Al₂O₃ confirms that it is a low-compressible material, whereas the relatively low ratio of the shear modulus to bulk modulus shows that it is still intrinsically brittle, somewhat more than θ -Al₂O₃. The shear strengths of θ -Al₂O₃ is much lower than that of α -Al₂O₃ due to the highly ionic Al-O bonds with the longest bond length that is more profound for θ -Al₂O₃. The longest Al-O bond lengths determine the deformation paths in both Al₂O₃ polymorphs.

ACKNOWLEDGEMENT

This research is sponsored by National Basic Research Program (973 Program) of China under grant No. 2012CB625100, National High-tech R&D Program (863 project) with No. 2012AA03A512, and Nature Science Foundations of China (NFSC) under grant No. 51231001 and No. 51425102. R.F. Zhang is supported by the Fundamental Research Funds for the Central Universities, NFSC with No. 51471018, and National Thousand Young Talents Program of China. D. Legut acknowledges financial and computational support by the IT4 Innovations Centre of Excellence project (CZ.1.05/1.1.00/02.0070), funded by the European Regional Development Fund and the national budget of the Czech Republic (project Large Research, Development and Innovations Infrastructures LM2011033). We would like to thank Prof. Dr. Stan Veprek for constructive comments and suggestions, and Prof. G. Kresse

for valuable advice for the application of VASP.

References

- [1] N. P. Padture, M. Gell and E.H. Jordan, *Science*, 2002, **296**, 280.
- [2] A. Stierle, F. Renner, R. Streitl, H. Dosch, W. Drube and B.C. Cowie, *Science*, 2004, **303**, 1652.
- [3] G. Kresse, M. Schmid, E. Napetschnig, M. Shishkin, L. Köhler and P. Varga, *Science*, 2005, **308**, 1440.
- [4] Z. Łodziana, N. Y. Topsoe and J.K. Norskov, *Nat. Mater.*, 2004, **3**, 289.
- [5] A. Erba, J. Maul, R. Demichelis, R. Dovesi, *Phys. Chem. Chem. Phys.*, 2015, **17**, 11670-11677.
- [6] M. F. Peintinger, M.J. Kratz, T. Bredow, *J. Mater. Chem. A*, 2014, **2**, 13143-13158.
- [7] I. Levin, D. Brandon, *J. Am. Ceram. Soc.*, 1998, **81**, 1995-2012.
- [8] C. -K. Lee, E. Cho, H. -S. Lee, K. Seol, S. Han, *Phys. Rev. B*, 2007, **76**, 245110.
- [9] L. Miseur, M. Bouslama, M. Amamra, A. Kanaev, *Phys. Status Solidi - Rapid Res. Lett.*, 2013, **7**, 1026-1029.
- [10] J. M. McHale, A. Auroux, A. J. Perrota and A. Navrotsky, *Science*, 1997, **277**, 788.
- [11] K. M. N. Prasanna, A.S. Khanna and R. Chandra, *Oxidation of Metals*, 1996, **46**, 465-480.
- [12] J. Doychak and M. Rühle, *Oxidation of Metals*, 1989, **31**, 431-452.
- [13] S. H. Cai, S. N. Rashkeev, S. T. Pantelides and K. Sohlberg, *Phys. Rev. B*, 2003, **67**, 224104.
- [14] E. Schumann, *Oxidation of Metals*, 1995, **43**, 157-172.
- [15] D. M. Lipkin, D.R. Clarke, M. Hollatz, M. Bobeth and W. Pompe, *Corros. Sci.*, 1997, **39**, 231-242.
- [16] R. H. French, *J. Am. Ceram. Soc.*, 1990, **73**, 477.
- [17] S. D. Mo and W. Y. Ching, *Phys. Rev. B*, 1998, **57**, 15219.
- [18] B. D. Evans, G. J. Pogatshnik, Y. Chen, *Nucl. Instr. Meth. Phys. Res. B.*, 1994, **91**, 258-262.
- [19] S. L. Shang, Y. Wang and Z. K. Liu, *Appl. Phys. Lett.*, 2007, **90**, 101909.

- [20] J. R. Gladden, J. H. So, J. D. Maynard, P. W. Saxe and Y. L. Page, *Appl. Phys. Lett.*, 2004, **85**, 392.
- [21] D. B. Hovis, A. Reddy and A. H. Heuer, *Appl. Phys. Lett.*, 2006, **88**, 131910.
- [22] S. L. Shang, W. Y. Wang, Y. Wang, Y. Du, J.X. Zhang, D. Patel and Z.K. Liu, *J. Phys. Condens. Matter*, 2012, **24**, 155402.
- [23] Q. Li, D. Zhou, W. Zheng, Y. Ma and C. Chen, *Phys. Rev. Lett.*, 2015, **115**, 185502.
- [24] S. Ogata, J. Li and S. Yip, *Science*, 2002, **298**, 807-811.
- [25] R. F. Zhang, D. Legut, Z.H. Fu, S. Veprek, Q.F. Zhang and H.K. Mao, *Phys. Rev. B*, 2015, **92**, 104107.
- [26] R. F. Zhang, D. Legut, Z. J. Lin, Y. S. Zhao, H. K. Mao and S. Veprek, *Phys. Rev. Lett.*, 2012, **108**, 255502.
- [27] S. L. Shang, W. Y. Wang, B. C. Zhou, Y. Wang, K. A. Darling, L. J. Kecskes, S. N. Mathaudhu and Z. K. Liu, *Acta Mater.*, 2014, **67**, 168-180.
- [28] M. Jahnátek, J. Hafner and M. Krajčí, *Phys. Rev. B*, 2009, **79**, 224103.
- [29] M. Zhang, H. Yan, B. Zheng and Q. Wei, *Sci. Rep.*, 2015, **5**, 15481.
- [30] F. Liu, P. Ming and J. Li, *Phys. Rev. B*, 2007, **76**, 064120.
- [31] G. Kresse and J. Hafner, *Phys. Rev. B*, 1993, **48**, 13115.
- [32] G. Kresse and J. Furthmuller, *Phys. Rev. B*, 1996, **54**, 11169.
- [33] J. P. Perdew, K. Burke and M. Ernzerhof, *Phys. Rev. Lett.*, 1996, **77**, 3865.
- [34] J. Heyd, G. E. Scuseria and M. Ernzerhof, *J. Chem. Phys.*, 2003, **118**, 8207.
- [35] R. F. Zhang, S. H. Sheng and S. Veprek, *Appl. Phys. Lett.*, 2007, **90**, 191903.
- [36] R. F. Zhang, S. H. Sheng and S. Veprek, *Appl. Phys. Lett.*, 2007, **91**, 031906.
- [37] R. F. Zhang, S. Veprek and A. S. Argon, *Appl. Phys. Lett.*, 2007, **91**, 201914.
- [38] R. F. Zhang, S. H. Sheng and S. Veprek, *Appl. Phys. Lett.*, 2009, **94**, 121903.
- [39] R. F. Zhang, D. Legut, X. D. Wen, S. Veprek, K. Rajan, T. Lookman, H. K. Mao, and Y. S. Zhao, *Phys. Rev. B*, 2014, **90**, 094115.
- [40] L. Lutterotti and P. Scardi, *J. Appl. Crystallogr.*, 1990, **23**, 246-252.
- [41] E. Husson and Y. Repelin, *J. Solid State Chem.*, 1996, **33**, 1223-1231
- [42] Z. Łodziana and K. Parlinski, *Phys. Rev. B*, 2003, **67**, 174106.

- [43] H. Z. Yao, L. Z. Ouyang and W.Y. Ching, *J. Am. Ceram. Soc.*, 2007, **90**, 3194-3204.
- [44] R. S. Zhou and R. L. Snyder, *Acta Crystallogr., Sect. B: Struct. Sci.*, 1991, **47**, 617.
- [45] C. Wolverton and K.C. Hass, *Phys. Rev. B*, 2000, **63**, 024102.
- [46] A. F. Wright, *J. Appl. Phys.*, 1997, **82**, 2833.
- [47] S. Q. Wang and H. Q. Ye, *J. Phys.: Condens. Matter*, 2005, **17**, 4475.
- [48] G. B. Brook, in *Smithells Metals Reference Book*, 8, edited by E. A. Brandes, 1983.
- [49] M. Born, *Proc. Cambridge Philos. Soc.*, 1940, **36**, 160.
- [50] G. Xu, A. S. Argon and M. Ortiz, *Philos. Mag. A*, 1997, **75**, 341.
- [51] G. Xu, A. S. Argon and M. Ortiz, *Philos. Mag. A*, 1995, **72**, 415.
- [52] S. F. Pugh, *Philos. Mag.*, 1954, **45**, 823.
- [53] M. Mattesini, R. Ahuja and B. Johansson, *Phys. Rev. B*, 2003, **68**, 184108.
- [54] J. R. Rice, G. E. Beltz and Y. Sun, in *Topics in Fracture and Fatigue*, edited by A.S. Argon (Springer, New York, 1992), pp. 1-58.
- [55] J. Haines, J. M. Leger and G. Bocquillon, *Annu. Rev. Mater. Res.*, 2001, **31**, 1.
- [56] J. J. Gilman, *Electronic Basis of the Strength of Materials* (Cambridge University Press, United Kingdom, 2003), pp. 1-4 and 201-225.
- [57] R. F. W. Bader, *Atoms in Molecules - A Quantum Theory*, Oxford University Press, Oxford, 1990.
- [58] G. Henkelman, A. Arnaldsson and H. Jónsson, *Comput. Mater. Sci.*, 2006, **36**, 254.
- [59] J. R. Weber, A. Janotti, C.G. Van de Walle, *J. Appl. Phys.*, 2011, **109**, 033715.
- [60] S. Park, B. Lee, S.H. Jeon, S. Han, *Curr. Appl. Phys.*, 2011, **11**, S337-S340.

Table 1. The elastic constants (C_{11} , C_{12} , C_{13} , C_{33} , C_{44} , C_{66}), bulk moduli (B_V), Young moduli (E), shear moduli (G_V) (GPa), and Poisson ratio (ν) of α -Al₂O₃ and θ -Al₂O₃ compared with previous calculations and available experimental measurements.

Property	α -Al ₂ O ₃				θ -Al ₂ O ₃		
	This work	GGA	LDA	EXP.	This work	GGA	LDA
C_{11}	455.2	437.2 ^a ,451.5 ^b	476.8 ^a ,497.1 ^b	497.5 ^c ,497 ^d ,497.4 ^e	268.0	269.1 ^b	283.8 ^b
C_{22}					389.7	389.3 ^b	420.4 ^b
C_{33}	457.1	443.3 ^a ,454.9 ^b	476.6 ^a ,492.5 ^b	503.3 ^c ,501 ^d ,499.1 ^e	405.8	404.2 ^b	435.3 ^b
C_{44}	132.6	125.5 ^a ,131.7 ^b	145.5 ^a ,154.2 ^b	147.4 ^c ,147 ^d ,147.4 ^e	72.5	74.2 ^b	86.8 ^b
C_{55}					102.0	102.2 ^b	104.3 ^b
C_{66}	151.6	146.4 ^a	159.6 ^a		122.3	126.0 ^b	124.5 ^b
C_{12}	152.0	144.3 ^a ,148.4 ^b	157.6 ^a ,164.7 ^b	162.7 ^c ,163 ^d ,164.0 ^e	112.2	113.2 ^b	119.3 ^b
C_{13}	112.2	101.5 ^a ,107.6 ^b	119.4 ^a ,129.5 ^b	115.5 ^c ,116 ^d ,112.2 ^e	135.5	132.2 ^b	159.8 ^b
B_V	235.6	223.4 ^a ,231.7 ^b	246.9 ^a ,259.3 ^b	252.3 ^c	187.4	186.9 ^b	207.1 ^b
G_V	149.4	143.0 ^a ,149.3 ^b	158.5 ^a ,165.8 ^b	166.0 ^c	109.5	110.7 ^b	114.9 ^b
E	370.0	353.6 ^a ,	391.6 ^a	403.0 ^c	274.9		
ν	0.238	0.2362 ^a	0.2356 ^a	0.23 ^c	0.256		

^a Ref.[43], ^b Ref. [21], ^c Ref. [44], ^d Ref. [17], ^e Ref. [48]

Figure Captions:

FIG. 1 (Color online): Lattice topology and polyhedra of the (a) Hexagonal α -Al₂O₃ and (c) Monoclinic θ -Al₂O₃. In each polyhedron, one Al cation is bonded to six O anions for α -Al₂O₃, four or six O anions for θ -Al₂O₃ structures respectively. The surrounding bond arrangements and length neighbor to each O atom for (b) α -Al₂O₃ and (d) (e) θ -Al₂O₃. The large and small spheres represent the Al (cations) and O (anions) respectively. O₁, O₂, O₃ are the O atoms with different local coordinations.

FIG. 2 (Color online): The stress-strain curves calculated by *ab initio* DFT method for (a) α -Al₂O₃ and (b) θ -Al₂O₃ under various tension and shear deformations. Three tensile deformations are along crystallographic directions: $\langle 0001 \rangle$, $\langle \bar{1}2\bar{1}0 \rangle$ and $\langle 10\bar{1}0 \rangle$ for α -Al₂O₃ and $\langle 100 \rangle$, $\langle 010 \rangle$ and perpendicular to (001) for θ -Al₂O₃; the shear deformations are along: (0001) $\langle \bar{1}2\bar{1}0 \rangle$, (0001) $\langle 10\bar{1}0 \rangle$ and (10 $\bar{1}0$) $\langle \bar{1}2\bar{1}0 \rangle$ for α -Al₂O₃ and (100) $\langle 010 \rangle$, (001) $\langle 010 \rangle$ and (001) $\langle 100 \rangle$ for θ -Al₂O₃.

FIG. 3 (Color online): The isosurfaces of valence charge density difference (VCDD) of α -Al₂O₃ (a) equilibrium, (b) before and (c) after instability under shear deformation along the weakest (0001) $\langle \bar{1}2\bar{1}0 \rangle$ slip system, and those of θ -Al₂O₃ (d) equilibrium, (e) before and (f) after instability under shear deformation along the weakest (001) $\langle 010 \rangle$ slip system (i.e. τ_{yz}). The isosurfaces maps of the VCDD correspond to -0.014 electrons/Bohr³. Yellow color means negative value. The crystallographic directions of $\langle 010 \rangle$ and $\langle 001 \rangle$ of monoclinic θ -Al₂O₃ are parallel to the y and z axes in

Cartesian coordinate system respectively as represented in Fig. 3(d).

FIG. 4. (Color online): The calculated electronic density of state (DOS) for (a) α -Al₂O₃ and (b) θ -Al₂O₃ and the cross-sectional plot of the valence charge density difference (VCDD) for (c) α -Al₂O₃ and (d) θ -Al₂O₃ to indicate the VCDD between the longest Al-O bonds. The circled region indicates the charge depletion between the longest Al-O bonds for both Al₂O₃.

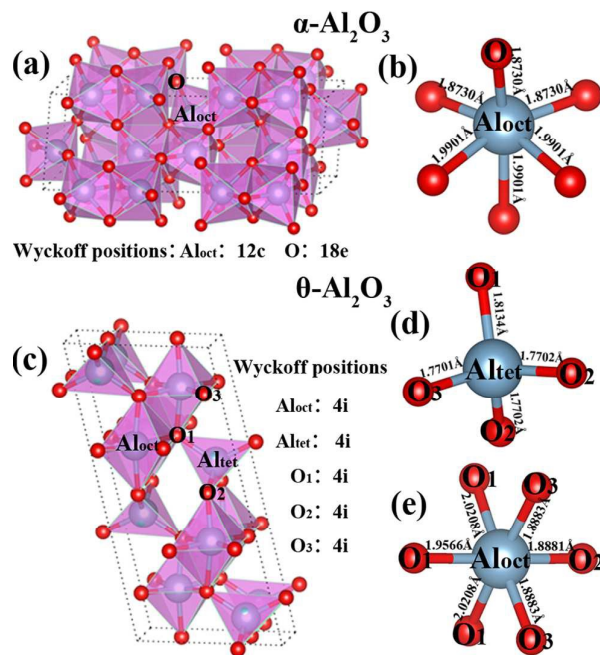


FIG. 1 (Color online): Lattice topology and polyhedra of the (a) Hexagonal $\alpha\text{-Al}_2\text{O}_3$ and (c) Monoclinic $\theta\text{-Al}_2\text{O}_3$. In each polyhedron, one Al cation is bonded to six O anions for $\alpha\text{-Al}_2\text{O}_3$, four or six O anions for $\theta\text{-Al}_2\text{O}_3$ structures respectively. The surrounding bond arrangements and length neighbor to each O atom for (b) $\alpha\text{-Al}_2\text{O}_3$ and (d) (e) $\theta\text{-Al}_2\text{O}_3$. The large and small spheres represent the Al (cations) and O (anions) respectively. O_1 , O_2 , O_3 are the O atoms with different local coordinations.

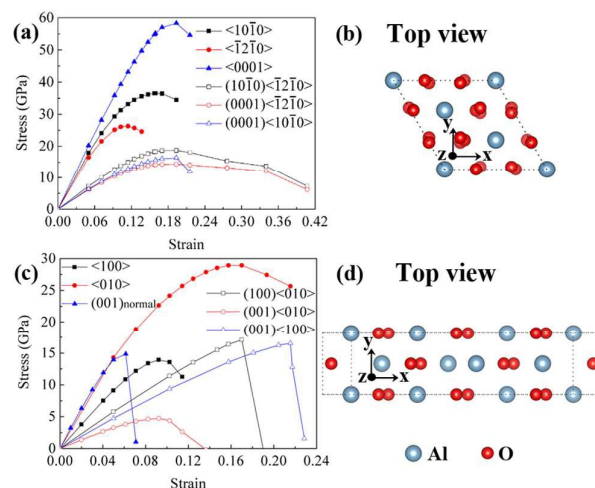


FIG. 2 (Color online): The stress-strain curves calculated by *ab initio* DFT method under various tension and shear deformations for (a) α -Al₂O₃ and (c) θ -Al₂O₃ and the top view structures for (b) α -Al₂O₃ and (d) θ -Al₂O₃. Three tensile deformations are along crystallographic directions: $\langle 0001 \rangle$, $\langle \bar{1}2\bar{1}0 \rangle$ and $\langle 10\bar{1}0 \rangle$ for α -Al₂O₃ and $\langle 100 \rangle$, $\langle 010 \rangle$ and perpendicular to (001) for θ -Al₂O₃; the shear deformations are along: $(0001)\langle \bar{1}2\bar{1}0 \rangle$, $(0001)\langle 10\bar{1}0 \rangle$ and $(10\bar{1}0)\langle \bar{1}2\bar{1}0 \rangle$ for α -Al₂O₃ and $(100)\langle 010 \rangle$, $(001)\langle 010 \rangle$ and $(001)\langle 100 \rangle$ for θ -Al₂O₃.

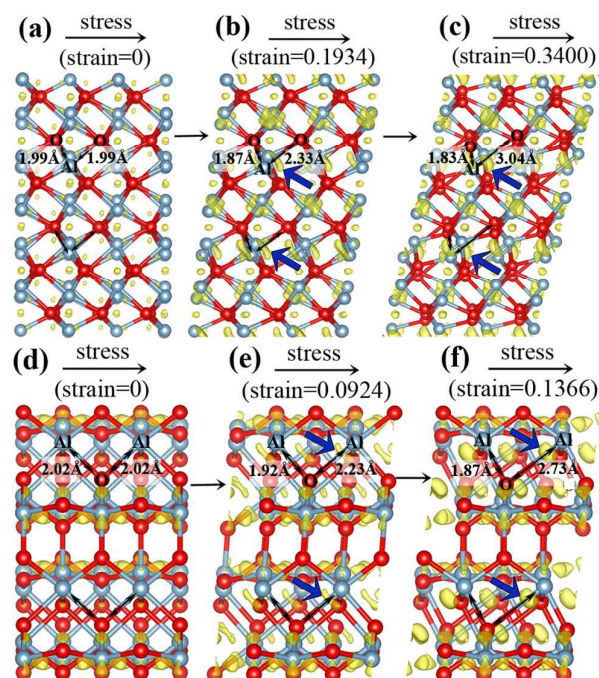


FIG. 3 (Color online): The isosurfaces of valence charge density difference (VCDD) of α - Al_2O_3 (a) equilibrium, (b) before and (c) after instability under shear deformation along the weakest $(0001)[\bar{1}2\bar{1}0]$ slip system, and those of θ - Al_2O_3 (d) equilibrium, (e) before and (f) after instability under shear deformation along the weakest $(001)[010]$ slip system (i.e. τ_{yz}). The isosurfaces maps of the VCDD correspond to -0.014 electrons/Bohr³. Yellow color means negative value. The crystallographic directions of $\langle 010 \rangle$ and $\langle 001 \rangle$ of monoclinic θ - Al_2O_3 are parallel to the y and z axes in Cartesian coordinate system respectively as represented in Fig. 2(d).

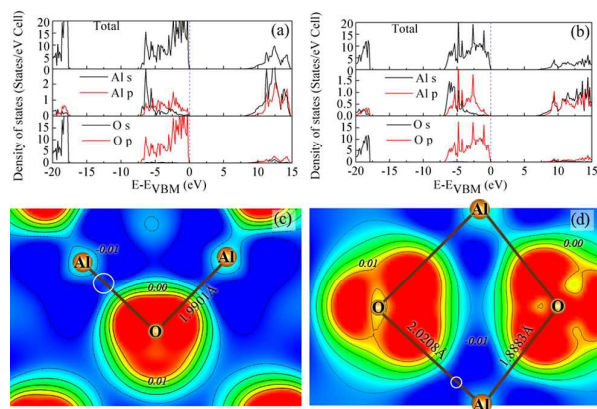
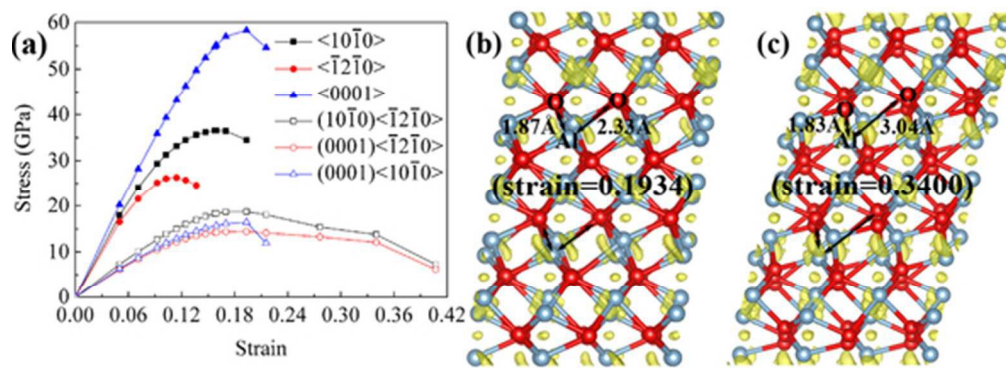


FIG. 4. (Color online): The calculated electronic density of state (DOS) for (a) α -Al₂O₃ and (b) θ -Al₂O₃ and the cross-sectional plot of the valence charge density difference (VCDD) for (c) α -Al₂O₃ and (d) θ -Al₂O₃ to indicate the VCDD between the longest Al-O bonds. The circled region indicates the charge depletion between the longest Al-O bonds for both Al₂O₃.



49x19mm (300 x 300 DPI)